Malaysian Journal of Chemistry, 2025, Vol. 27(3), 190-199
(Special Issue: *2nd International Science and Technology Colloquium, i-COSTECH 2024*)

Synthesis of CeO_2-Supported Gold Catalyst (Au-CeO_2) for *p*-Nitrophenol Reduction

Mohamad Zuhairi Abdul Rahman[1], Muhammad Firdaus Sahrullizam[1], Hanani Yazid[1]*, Nafisah Osman[1], Abdul Mutalib Md Jani[2] and Chung-Jen Tseng[3]
[1]Faculty of Applied Sciences, Universiti Teknologi MARA Perlis Branch, Arau Campus,
02600 Arau, Perlis, Malaysia
[2]Faculty of Applied Sciences, Universiti Teknologi MARA Perak Branch, Tapah Campus,
35400 Tapah Road, Perak, Malaysia
[3]Center for Energy Research, National Central University, 300 Zhongda Road, Zhongli District,
Taoyuan City 32001, Taiwan
*Corresponding author (e-mail: hanani946@uitm.edu.my)

The reduction of *p*-nitrophenol (*p*-NP) is widely used as a model reaction to evaluate catalytic activity. In this study, cerium oxide (CeO_2) supports were synthesized via two simple methods: chemical precipitation (method A) and co-precipitation (method B). Gold (Au) nanoparticles were subsequently deposited onto CeO_2 supports using the deposition-precipitation (DP) technique. The CeO_2 supports were prepared by reacting cerium nitrate with ammonia solution (method A) and potassium carbonate (method B), producing cerium oxide particles. The resulting particles were characterized using Fourier Transform Infrared (FTIR) spectroscopy. FTIR analysis revealed prominent peaks in the range of 3300–2800 cm^{-1}, corresponding to O-H stretching in CeO_2-A and CeO_2-B. X-ray diffraction (XRD) analysis confirmed the cubic fluorite structure of cerium oxide in both samples (JCPDS No. 01-075-0076). Meanwhile, the FTIR spectra of Au-CeO_2-A and Au-CeO_2-B demonstrated successful Au immobilization, as evidenced by shifts in the support's characteristic peaks. Inductively Coupled Plasma-Optical Emission Spectroscopy (ICP-OES) confirms the presence of Au, with loadings of 0.565 wt% in Au-CeO_2-A and 0.465 wt% in Au-CeO_2-B, respectively. The Au-CeO_2 catalysts achieved 100% conversion of *p*-NP to *p*-aminophenol, with a rate constant (k) of 5.78×10^{-4} s^{-1} for Au-CeO_2-A and 4.37×10^{-4} s^{-1} for Au-CeO_2-B.

Keywords: Cerium oxide (CeO_2); gold (Au); deposition-precipitation; *p*-nitrophenol (*p*-NP)

Received: October 2024; Accepted: December 2024

Cerium oxide (CeO_2) is a versatile metal oxide known for its ability to switch between two oxidation states: Ce (III) and Ce (IV). It also features a high oxygen storage capacity, a large surface area, high reactivity, and thermal stability. These properties are particularly enhanced when CeO_2 is in nanoparticle form [1]. This makes CeO_2 a valuable material for various applications, including fuel cell electrodes, UV protection, and catalysis. Specifically, CeO_2 serves as an effective catalyst in oxidation and reduction reactions [2]. Additionally, CeO_2 is commonly used as a support for noble metals such as gold (Au), silver (Ag), and palladium (Pd) in catalytic processes, where it enhances the stability and efficiency of these metals in various chemical reactions, including the reduction of *p*-nitrophenol (*p*-NP) [3].

The synthesis of CeO_2 using cerium nitrate as a precursor in methods like hydrothermal treatment and sol-gel faces several challenges [4, 5]. These include high costs, elevated operating pressures, and temperatures, as well as prolonged reaction times. Additionally, different preparation methods have been reported to produce CeO_2 particles with varying purity and size. Particularly, methods that involve stabilizers or capping agents can compromise the purity of the final product [6, 7].

In this study, chemical precipitation and co-precipitation were chosen as the preparation methods due to their simplicity and cost-effectiveness [8]. These methods have been shown to produce CeO_2 nanoparticles with sizes below 100 nm, which is advantageous as nanoscale CeO_2 exhibits a higher surface area. A high surface area support is particularly effective for depositing metal nanoparticles such as Au as it provides more active sites for the reaction to occur [9]. Several studies have reported the use of Au-CeO_2 catalysts in various chemical reactions, demonstrating high activity depending on factors such as Au particle size, preparation method, and Au loading [10-12]. Besides, the use of CeO_2 synthesized by different methods can also impact the catalyst's performance. Thus, this study aims to investigate the effect of different CeO_2 supports on the catalytic activity of Au-CeO_2 in the reduction of *p*-nitrophenol (*p*-NP).

---

†Paper presented at the 2nd International Science and Technology Colloquium (i-COSTECH 2024)

The *p*-NP is a prevalent organic compound found in wastewater from industries such as pharmaceuticals, paper, pesticides, and plastics [13]. Due to its potential to cause various health problems, including inflammation, coughing, a burning sensation, and rapid heartbeat, it poses significant risks to human health. Furthermore, *p*-NP has a considerable environmental impact, making its effective treatment and management crucial for both ecological and public health reasons [14]. Particularly, the catalytic reduction of *p*-NP offers significant advantages over other methods, such as adsorption and degradation, as it generates *p*-aminophenol, an important intermediate in the synthesis of analgesic drugs [15-17].

EXPERIMENTAL

Chemicals and Materials

A high-purity (99% purity) cerium nitrate hexahydrate ($Ce(NO_3)_3.6H_2O$), potassium carbonate (K_2CO_3), gold(III) chloride trihydrate ($HAuCl_4.3H_2O$), and sodium hydroxide (NaOH) were supplied by Sigma-Aldrich (USA). Aqueous ammonia solution (NH_4OH), and ethanol (C_2H_6O, 95%) were obtained from a commercial supplier, HmbG Chemical. *p*-Nitrophenol (*p*-NP) was acquired from Merck (Darmstadt, Germany). Lastly, sodium borohydride ($NaBH_4$) was purchased from Friendemann Schmidt.

Preparation of CeO_2 by Chemical Precipitation

Cerium oxide was prepared by dissolving 150 mL of 0.1 M cerium nitrate hexahydrate (99%, purity, ($Ce(NO_3)_3.6H_2O$, Sigma-Aldrich,), in 50 mL of deionized water and stirring vigorously for 30 minutes. Meanwhile, 25 mL of aqueous ammonia solution, (NH_4OH, HmbG Chemical) was added dropwise over 20 minutes and the mixture was stirred for 15 hours at room temperature. After the ammonia was added to the cerium nitrate solution, a significant colour change was observed. During the first 10 minutes, the slurry was light brown at low pH, likely due to the presence of Ce^{3+}. After 2 hours, it turned light white-black, followed by a transition to brown at 3 hours, then orange at 5 hours, and finally light yellow due to the formation of Ce^{4+} in the presence of oxygen. The resulting slurry was filtered and washed several times with deionized water and ethanol. Subsequently, the precipitate was then dried in an oven at 60 °C for 3 hours. After drying, the powder was ground for 15 minutes using a mortar and pestle and annealed at 450 °C for 2 hours to enhance the crystallinity of the samples. The sample is denoted as CeO_2-A.

Preparation of CeO_2 by Co-precipitation Method

Cerium oxide was prepared using cerium nitrate hexahydrate, $Ce(NO_3)_3·6H_2O$ (99%, Sigma-Aldrich) as the precursor. Aqueous solutions of Ce (III) nitrate (0.02 M, 500 mL) and potassium carbonate (0.03 M, 200 mL) were added drop by drop to a well-stirred 500 mL of water to precipitate a white precursor, cerium (III) carbonate. Sodium hydroxide, 1 M was used to adjust the pH to 8. The resulting CeO_2 was dried at 65 °C for 2 hours and then cooled to room temperature. Subsequently, the product was aged for 2.5 hours at 220 °C without washing or purification before being calcined for 3 hours at 800 °C [8]. The sample is denoted as CeO_2-B.

Preparation of Au-CeO_2-A and Au-CeO_2-B by Deposition-precipitation Method

Gold (III) chloride trihydrate, $HAuCl_4.3H_2O$ (0.004 M, 100 mL) solution was heated to 80 °C. NaOH (Sigma-Aldrich) was added drop by drop to adjust the pH to the desired level of 8. Approximately 0.5 grams of CeO_2 support were then dispersed in the solution, causing a pH change. The pH was maintained at a constant level by slowly adding 0.25 M NaOH. The suspension was kept at 80 °C and stirred vigorously for 2 hours. The resulting precipitates obtained were washed several times to remove residual sodium and chloride ions, as well as untreated Au species. Finally, the precipitates were centrifuged and dried at 400 °C for 4 hours to allow the decomposition of gold precursors into their metallic state [18].

Characterization Methods

The surface properties of CeO_2 support and Au-CeO_2 were analyzed using the Fourier Transform Infrared spectrometer, FTIR (Frontier, Perkin Elmer) equipped with an Attenuated Total Reflectance (ATR). The samples were characterized over a scanning range of 4000-600 cm^{-1}. Meanwhile, X-ray diffraction (XRD) analysis was performed using an X'Pert Pro diffractometer (PANanalytical) to examine the crystalline properties and purity of the synthesized CeO_2. The characterization was carried out at 45 kV, scanning two-theta (θ) angles from 20° to 80°. The CeO_2-A and CeO_2-B samples were also examined using Scanning Electron Microscopy (SEM, JEOL). A small amount of each sample was placed on carbon tape and coated with a thin layer of platinum. The SEM operational parameters were set to 5 kV, with a working distance of 6.8 mm, allowing for magnification up to 50,000×. The samples were then subjected to an electron beam, and the resulting images were recorded for detailed analysis. Finally, the gold (Au) loading in both Au-CeO_2-A and Au-CeO_2-B was determined using an Inductively Coupled Plasma Optical Emission Spectrometer (ICP-OES, Optima 8000, Perkin Elmer). For the ICP-OES analysis, the catalysts were first digested in aqua regia, then diluted with deionized water, and filtered through a 0.45 µm membrane filter before analysis. The Au content (wt.%) was calculated using the formula: Au (%wt) = (mass of Au) / (mass of catalyst) × 100 [19].

Catalytic Study

Dissolve 0.0139 g of recrystallized *p*-nitrophenol (*p*-NP) (99%, MERCK) in 10 mL deionized water. Then, dilute 250 µL of this solution in a 50 mL volumetric flask. For sodium borohydride ($NaBH_4$), dissolve 0.0473 g in 25 mL deionized water. Then 15 mL of this solution was diluted in a 50 mL volumetric flask. Finally, pipette 1.5 mL of the $NaBH_4$ (15.0 mM) solution into a cuvette and add 1 mg of $Au-CeO_2$-A, followed by 1.5 mL of the prepared *p*-NP (0.05 mM). Shake the mixture three times and immediately begin the catalytic study using UV-Vis. Similar procedures were repeated for $Au-CeO_2$-B and CeO_2 (controlled). The catalytic reaction was evaluated by monitoring the decrease of absorbance overtime at 400 nm using a UV-Vis spectrophotometer (Lambda 25, Perkin Elmer). The rate constant (k) was calculated based on the pseudo-first-order kinetics from the plot ln (A/A_o) vs. time.

RESULTS AND DISCUSSION

CeO_2 Nanoparticle

Figure 1 shows CeO_2 powder synthesized by two different methods chemical precipitation and co-precipitation after calcination. During the synthesis, a notable color change in the solution was observed. Initially, the slurry appeared purple at a low pH, then transitioned to brown at an intermediate pH, and finally turned to yellow or pale yellow at a higher pH. This color transition was consistent for techniques A (chemical precipitation) and B (co-precipitation), with the pH stabilized at 8 throughout the process [20]. The color change during the synthesis of CeO_2 is important because it reveals changes in the chemical and structural properties of the material. Cerium oxide can exist in different oxidation states, which produce different colors. The color shift during synthesis often indicates changes in the oxidation state of cerium and the formation of CeO_2 nanoparticles [21].

Table 1 tabulates the percentage of yield of CeO_2 obtained using methods A and B. The percentage yield is calculated as the ratio of the actual yield to the theoretical yield, multiplied by 100%. A 100% yield indicates that the actual yield matches the theoretical yield. The percentage yield for CeO_2-A and CeO_2-B were 91.08% and 109.77%, respectively. These results show variation: method A produced a yield less than 100%, while method B exceeded 100%. This discrepancy may be due to incomplete reactions, sample loss, or experimental inconsistencies.

FTIR spectroscopy was used to characterize the surface properties of the prepared CeO_2-A and CeO_2-B samples. The spectra were recorded to examine the vibrational behavior and confirm the presence of CeO_2 through distinct vibrational peaks. **Figure 2** shows the FTIR spectra of CeO_2-A and CeO_2-B, recorded using an FTIR spectrometer (Frontier, Perkin Elmer) in the range of 600 to 4000 cm^{-1}. An intense band observed at 3300 - 2800 cm^{-1} in both samples corresponds to O-H stretching [22]. CeO_2-A showed clearer peak separation than CeO_2-B, resulting from the different concentrations of the O-H group in the sample. The weak intensity band of CeO_2-A was detected at 2885 cm^{-1}, corresponding to C-H vibrations, while these peaks were absent in CeO_2-B. Additional bands in the 1628-1000 cm^{-1} range (C-O bond) are likely due to the presence of residual or the formation of "carbonate-like" species on the ceria surface [23].

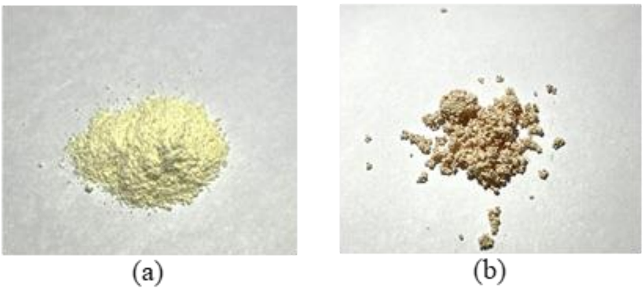

Figure 1. Photograph of (a) CeO_2-A and (b) CeO_2-B.

Table 1. The percentage yield of CeO_2 prepared by method A and B.

Method	Notation	Theoretical yield (g)	Actual yield (g)	Percentage yield (%)
Chemical precipitation (A)	CeO_2-A	2.581	2.351	91.08
Co-precipitation (B)	CeO_2-B	1.033	1.134	109.77

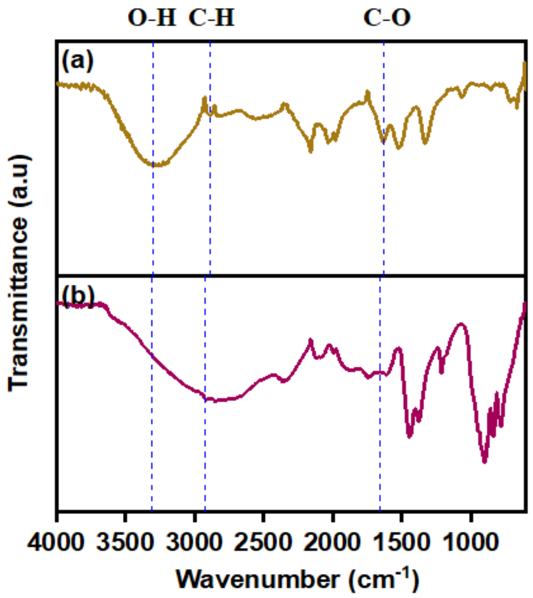

Figure 2. FTIR spectra of (a) CeO_2-A and (b) CeO_2-B.

The structural identification of cerium oxide was performed using X-ray diffraction in the 2θ range between 20° and 95°, as shown in **Figure 3**. The XRD results revealed distinct diffraction peaks associated with CeO_2 in all samples at 2θ angles of 28.67°, 33.23°, 47.69°, 56.60°, 59.36°, 69.75°, 77.08°, 79.47° and 88.90° (JCPDS No. 01-075-0076). These peaks correspond to the Fm-3m space group, confirming the cubic structure for both samples. The observed peaks indicate clear evidence of the crystalline nature and structural integrity of the synthesized CeO_2. Both CeO_2-A and CeO_2-B show very slight differences in the peak positions, indicating that both methods successfully produce pure CeO_2. Additionally, no extraneous peaks were observed, confirming the absence of impurities in the synthesized samples. The higher intensity of the peaks for CeO_2-B suggests a greater number of atoms in the crystal lattice, indicating a higher degree of crystallinity, or a larger crystal size compared to CeO_2-A, which exhibits shorter and broader peaks [24].

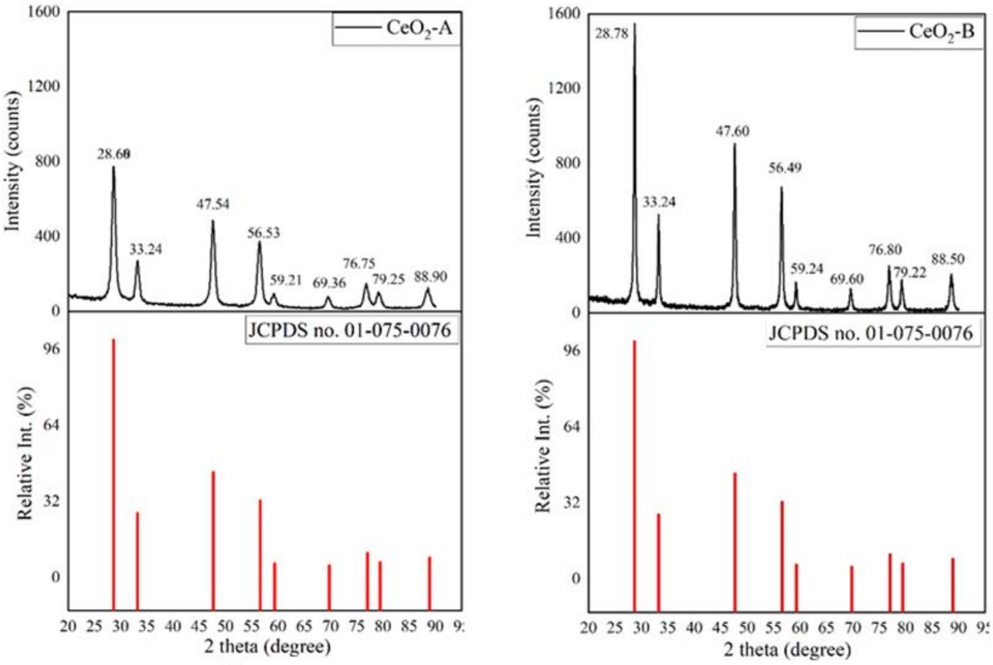

(a) (b)

Figure 3. XRD pattern for (a) CeO_2-A and (b) CeO_2-B and the corresponding diffraction pattern from JCPDS No. 01-075-0076.

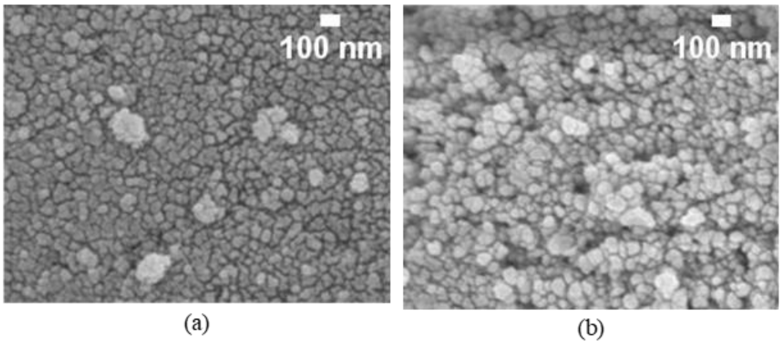

Figure 4. SEM images of (a) CeO_2-A and (b) CeO_2-B.

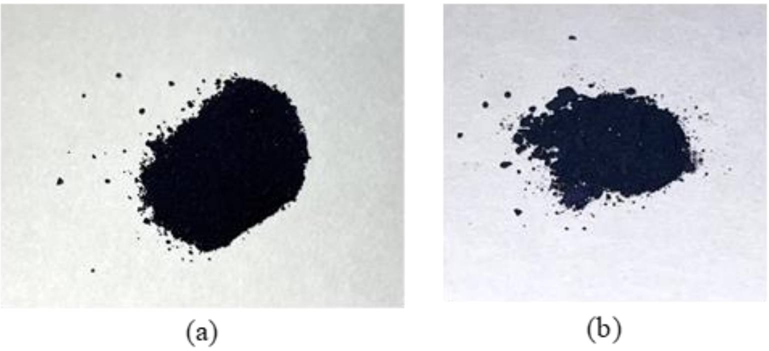

Figure 5. Photograph of (a) Au-CeO_2-A and (b) Au-CeO_2-B.

Figure 4 presents SEM images used to analyze the morphology of the synthesized CeO_2. The analysis reveals that neither sample exhibited significant agglomeration, and both retained a spherical morphology. Using ImageJ software, the average diameter of CeO_2 nanoparticles was determined, with samples synthesized by chemical precipitation and co-precipitation having average diameters of 55.75 nm and 72.57 nm, respectively. SEM is particularly effective for studying the microstructure of catalyst materials, providing high-resolution imaging at the nanoscale [25].

Au-CeO_2 Catalyst

Figure 5 shows photographs of Au-CeO_2-A and Au-CeO_2-B, both of which exhibited a dark purple color [26]. These changes indicate that Au was successfully reduced following calcination at 400°C. Bond et al. state that the interaction between the electrons of the Au 5d orbitals and the cations from the support contribute to the observed color change [27]. However, this is not the only factor [28, 29]. The color of supported Au nanoparticles is also influenced by factors such as particle size, concentration, morphology, and size distribution, as reported by Galvagno and Parravano [30]. These color variations reflect the metallic character of Au (Au^0), and color assessment can serve as a preliminary method for identifying Au^0 in the samples. Since both Au-CeO_2 exhibit a dark purple color, suggesting that the Au NPs are likely within a similar size range. According to the literature, the particle size typically falls within the range of 10-20 nm [31]. ICP-OES results show that the Au loadings in Au-CeO_2-A and Au-CeO_2-B are 0.565 wt.% and 0.465 wt.%, respectively.

Figure 6 displays the FTIR spectra for (a) Au-CeO_2-A and (b) Au-CeO_2-B against CeO_2-A and CeO_2-B, respectively. Shifting of the O-H peak occurs from 3421 cm^{-1} in CeO_2-A to 3270 cm^{-1} in Au-CeO_2-A. Notably, the C-O stretching vibration (from adsorbed carbon monoxide) in Au-CeO_2-A exhibits a significant decrease in intensity at 2160 cm^{-1}, while other peaks show no significant change in intensity. A similar trend was observed in CeO_2-B compared to Au-CeO_2-B. The O-H peak for CeO_2-B appeared at 3185 cm^{-1}, while in Au-CeO_2-B, the peak was observed at 2815 cm^{-1}. The shifting of some FTIR peaks in the Au-CeO_2 sample suggests that Au crystallites have been effectively incorporated into the CeO_2 lattice and are well-distributed across the CeO_2 support [32, 33]. Therefore, it can be concluded that the Au has been successfully deposited onto both CeO_2 supports.

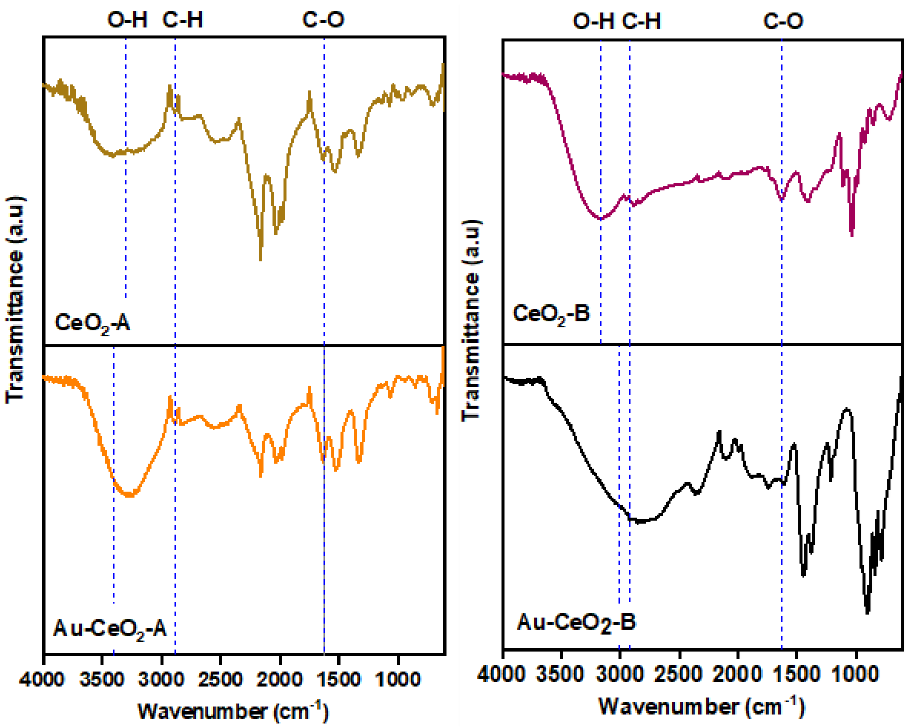

(a) (b)

Figure 6. FTIR spectra of (a) $Au-CeO_2$-A and (b) $Au-CeO_2$-B.

Catalytic Reduction of *p*-Nitrophenol

The catalytic activities of the $Au-CeO_2$-A and $Au-CeO_2$-B catalysts were assessed through the reduction of *p*-NP to *p*-aminophenol (*p*-AP) in the presence of $NaBH_4$ at room temperature. According to Liu, the primary absorption peak of the *p*-NP solution occurs at 317 nm. However, in the presence of excess $NaBH_4$, the solution exhibits a strong absorbance peak at 400 nm, which corresponds to the *p*-nitrophenolate ion [34]. The progress of the reaction was monitored by UV-Vis spectroscopy, and the decrease in the intensity of the *p*-nitrophenolate ion peak over time reflects the successful reduction of *p*-NP. In the presence of CeO_2 support alone (control), the reduction of *p*-NP does not occur, resulting in no change in absorbance at 400 nm and the persistent bright yellow color of the solution. Conversely, as shown in **Figure 7(a)** the addition of $Au-CeO_2$ results in a rapid decrease in absorbance at 400 nm, indicating that the reduction of *p*-NP has occurred, as shown in the absorbance vs. time plot. Additionally, the inset image in **Figure 7(a)** shows a photograph of the *p*-NP solution before and after the catalytic reaction over $Au-CeO_2$-A catalyst. The solution changes from bright yellow to colorless, further confirming the complete conversion of *p*-NP to *p*-AP [35, 36].

The catalytic reduction of *p*-NP follows pseudo-first-order kinetics, allowing the rate constant (*k*) to be calculated from the slope of $\ln (A/A_o)$ plot. **Figure 7(b)** illustrates this plot for $Au-CeO_2$-A and $Au-CeO_2$-B. The highest *k* value of 5.78×10^{-4} s^{-1} was obtained $Au-CeO_2$-A while the $Au-CeO_2$-B catalyst had a rate constant of 4.37×10^{-4} s^{-1}. The influence of support particle size on catalytic performance is particularly evident when comparing the two ceria supports, CeO_2-A and CeO_2-B. CeO_2-A has a smaller particle size, which results in a higher surface area and provides more active sites for the reactants, leading to more efficient adsorption and improved interaction between the catalyst and the reactants [9]. According to Zheng and co-workers, the decrease in nanoparticle size is a significant factor influencing the reaction rate [37].

Additionally, smaller support particles typically exhibit a higher density of exposed surface atoms, which can more effectively stabilize the Au nanoparticles, facilitating faster electron transfer and more efficient reaction pathways [38]. As a result, reactions occur at a faster rate, highlighting the critical role of support particle size in influencing catalytic activity [39]. Furthermore, these results align with the ICP-OES data, which show that the Au loading in $Au-CeO_2$-A is higher than in $Au-CeO_2$-B, contributing to better catalytic activity.

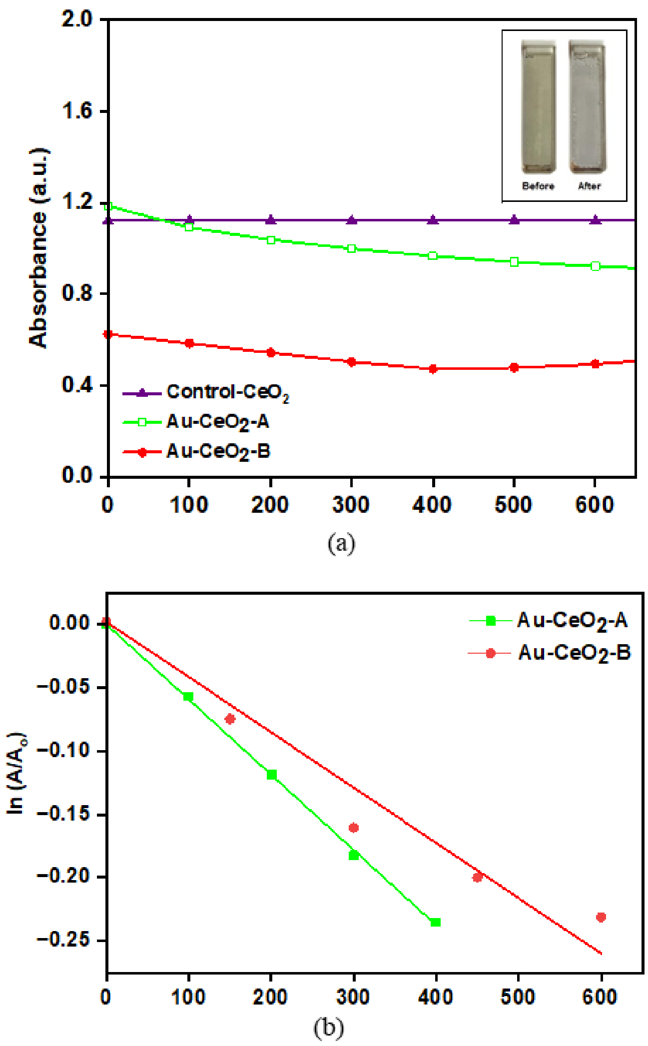

Figure 7. (a) Graph absorbance vs time for Au-CeO_2-A, Au-CeO_2-B, and CeO_2-control. The inset image is the photograph of the *p*-NP solution before and after the catalytic reaction and (b) Plot ln(A/A_o) vs time for *p*-NP reduction over for Au-CeO_2-A and Au-CeO_2-B catalyst.

Table 2. The CeO_2 particle size, Au loadings, reaction time and *k* value of Au-CeO_2 catalysts prepared by chemical precipitation and co-precipitation methods.

Catalyst	CeO_2 Preparation Method	CeO_2 Particle Size (nm)	Au loadings (wt%)	Reaction time (s)	*k*-value (s^{-1})
Au-CeO_2-A	Chemical- precipitation	55.75	0.565	400	5.78 x 10^{-4}
Au-CeO_2-B	Co-precipitation	73.57	0.465	600	4.37 x 10^{-4}

Concerning the size of gold (Au) particles, previous research has confirmed that the deposition-precipitation (DP) method at pH 8 yields Au particles smaller than 20 nm. Since both samples were prepared under the same pH conditions using the DP method, we anticipate the Au particle sizes to be comparable. **Table 2** summarizes the support particle size, Au loading, reaction time, and *k* value of the prepared Au-CeO_2 catalysts.

The investigation into catalytic activities involved calculating and comparing the *k* values of the reported method with those of other catalysts from various studies. A comparison of Au on metal oxide catalysts is provided in **Table 3**. These findings highlight potential avenues for future research aims at further optimizing the performance of Au-CeO_2 in the reduction of *p*-NP.

Table 3. Comparison of rate constant of catalytic reduction of different catalyst.

Catalyst	Catalyst rate constant (*k*) value	References
Au/TNT	0.61×10^{-4}	[40]
Au/ANT	0.50×10^{-4}	[40]
Au-CA	0.50×10^{-3}	[41]
Au/Al_2O_3	6.80×10^{-3}	[42]

CONCLUSION

In conclusion, cerium oxide supports were successfully synthesized using co-precipitation and chemical precipitation methods, resulting in effective deposition of gold (Au) on both supports. Characterization of the samples was performed using FTIR and XRD techniques. FTIR analysis revealed prominent peaks at 3300-2800 cm^{-1} in both samples corresponding to O-H stretching. XRD analysis confirmed that the diffraction peaks matched those of CeO_2, consistent with the reference pattern (JCPDS No. 01-075-0076), indicating the presence of pure CeO_2 with a cubic fluorite structure. Additionally, FTIR analysis of $Au-CeO_2$-A and $Au-CeO_2$-B further confirmed the successful immobilization of Au on CeO_2, as evidenced by the shifting of O-H stretching peaks. The catalytic performance of both catalysts showed 100% conversion to *p*-aminophenol, with rate constants (*k*) of 5.78×10^{-4} s^{-1} for $Au-CeO_2$-A and 4.37×10^{-4} s^{-1} for $Au-CeO_2$-B. Based on these results, the catalyst prepared using the chemical precipitation method ($Au-CeO_2$-A), demonstrated better performance compared to the catalyst produced by the co-precipitation method. Future research to enhance this study should include investigating the long-term stability and reusability of the catalysts, as well as conducting detailed mechanistic studies to gain deeper insights into the catalysts' behavior and efficiency.

ACKNOWLEDGEMENTS

The authors gratefully acknowledge the support from the Universiti Teknologi MARA Perlis Branch, Arau, Malaysia, and the Center for Energy Research, National Central University (NCU), Taiwan for the matching grant: 100-TNCPI/INT 16/6/2 (065/2023)

REFERENCES

1. Dhall, A. and Self, W. (2018) Cerium oxide nanoparticles: a brief review of their synthesis methods and biomedical applications. *Antioxidants*, **7**, 97–110.

2. Singh, K. R., Nayak, V., Sarkar, T. and Singh, R. P. (2020) Cerium oxide nanoparticles: properties, biosynthesis and biomedical application. *RSC Advances*, **10**, 27194–27214.

3. Xu, X., Li, M., Yang, L. and Hu, B. (2023) Remarkably and stable catalytic activity in reduction of 4-nitrophenol by sodium sesquicarbonate-supporting Fe_2O_3@Pt. *RSC Advances*, **13**, 13556–13563.

4. Gatea, H.A. (2022) Effect of high temperature on thermal analysis, structure and morphology of CeO_2 nanoparticles prepared by hydrothermal method. *International Journal of Thin Film Science and Technology*, **11**, 201–210.

5. Fudala, A. S., Salih, W. M. and Alkazaz, F. F. (2022) Synthesis different sizes of cerium oxide CeO_2 nanoparticles by using different concentrations of precursor via sol–gel method. *Materials Today: Proceedings*, **49**, 2786–2792.

6. Nyoka, M., Choonara, Y., Kumar, P., Kondiah, P. and Pillay, V. (2020) Synthesis of cerium oxide nanoparticles using various methods: implications for biomedical applications. *Nanomaterials*, **10**, 1–21.

7. Nosrati, H., Heydari, M. and Khodaei, M. (2023) Cerium oxide nanoparticles: synthesis methods and applications in wound healing. *Materials Today Bio*, **23**, 1–25.

8. Farahmandjou, M., Zarinkamar, M. and Firoozabadi, T. (2016) Synthesis of cerium oxide (CeO_2) nanoparticles using simple co-precipitation method. *Revista Mexicana de Física*, **62**, 496–499.

9. Quan, Y. -H., Chao, M., Tao, L., Na, W., Wu, M. -M., Zhang, N., Zhao, J. -X. and Jun, R. (2021) Effect of preparation methods on the structure and catalytic performance of CeO_2 for toluene combustion. *Journal of Fuel Chemistry and Technology*, **49**, 211–219.

10. Centeno, M. A., Ramírez Reina, T., Ivanova, S., Laguna, O. H. and Odriozola, J. A. (2016) Au/CeO_2 catalysts: structure and CO oxidation activity. *Catalysts*, **6**, 158–168.

11. Jinwei, L. and Weibin, L. (2010) Effect of preparation method on the catalytic activity of Au/CeO_2 for VOCs oxidation. *Journal of Rare Earths*, **28**, 547–551.

12. Han, M., Wang, X., Shen, Y., Tang, C., Li, G. and Smith Jr., R. L. (2010) Preparation of highly active, low Au-loaded, Au/CeO_2 nanoparticle catalysts that promote CO oxidation at ambient temperatures. *Journal of Physical Chemistry C*, **114**, 793–798.

13. Maszenan, A., Liu, Y. and Ng, W. J. (2011) Bioremediation of wastewaters with recalcitrant organic compounds and metals by aerobic granules. *Biotechnology Advances*, **29**, 111–123.

14. Ho, T. G. -T., Do, B. L., Van Pham, B., Van Nguyen, T. T., Phan, H. P., Nguyen, H. B., Vo, P. P. T. and Tri, N. (2022) High-efficiency reduction of p-nitrophenol on green-synthesized gold nanoparticles decorated on ceria nanorods. *RSC Advances*, **12**, 25753–25763.

15. Qin, Y., Luo, J., Zhao, Y., Yao, C., Li, Y., An, Q., Xiao, Z. and Zhai, S. (2022) Dual-wastes derived biochar with tailored surface features for highly efficient *p*-nitrophenol adsorption. *Journal of Cleaner Production*, **353**, 131571–113189.

16. Rodrigues, C. S. and Madeira, L. M. (2021) *p*-Nitrophenol degradation by activated persulfate. *Environmental Technology & Innovation*, **21**, 101265–101279.

17. Panda, S. S., Girgis, A. S., Honkanadavar, H. H., George, R. F. and Srour, A. M. (2020) Synthesis of new ibuprofen hybrid conjugates as potential anti-inflammatory and analgesic agents. *Future Medicinal Chemistry*, **12**, 1369–1386.

18. Yazid, H., Rahman, N. A. A. and Jani, A. M. M. (2021) Catalytic reduction of p-nitrophenol on Au/TiO_2 powder and Au/TiO_2 membrane. *AIP Conference Proceedings, AIP Publishing LLC*, 1–10.

19. Moreau, F. and Bond, G. C. (2007) Preparation and reactivation of Au/TiO_2 catalysts. *Catalysis Today*, **122**, 260–265.

20. Zhou, X. -D., Huebner, W. and Anderson, H. U. (2003) Processing of nanometer-scale CeO_2 particles. *Chemistry of Materials*, **15**, 378–382.

21. Charbgoo, F., Ahmad, M. B. and Darroudi, M. (2017) Cerium oxide nanoparticles: green synthesis and biological applications. *International Journal of Nanomedicine*, **12**, 1401–1413.

22. Suresh, R., Ponnuswamy, V. and Mariappan, R. (2013) Effect of annealing temperature on the microstructural, optical and electrical properties of CeO_2 nanoparticles by chemical precipitation method. *Applications of Surface Science*, **273**, 457–464.

23. Liu, S., Qileng, A., Huang, J., Gao, Q. and Liu, Y. (2017) Polydopamine as a bridge to decorate monodisperse gold nanoparticles on Fe_3O_4 nanoclusters for the catalytic reduction of 4-nitrophenol. *RSC Advances*, **7**, 45545–45551.

24. Prabaharan, D. D. M., Sadaiyandi, K., Mahendran, M. and Sagadevan, S. (2018) Investigating the effect of Mn-doped CeO_2 nanoparticles by co-precipitation method. *Applied Physics A*, **124**, 86–100.

25. Phokha, S., Pinitsoontorn, S., Chirawatkul, P., Poo-Arporn, Y. and Maensiri, S. (2012) Synthesis, characterization, and magnetic properties of monodisperse CeO_2 nanospheres prepared by PVP-assisted hydrothermal method. *Nanoscale Research Letters*, **7**, 1–13.

26. Tran, N. D., Besson, M., Descorme, C., Fajerwerg, K. and Louis, C. (2011) Influence of the pretreatment conditions on the performances of CeO_2-supported gold catalysts in the catalytic wet air oxidation of carboxylic acids. *Catalysis Communications*, **16**, 98–102.

27. Bond, G. C. and Thompson, D. T. (1999) Catalysis by gold. *Catalysis Reviews-Science and Engineering*, **41**, 319–388.

28. Carltonbird, M., Eaimsumang, S., Pongstabodee, S., Boonyuen, S., Smith, S. M. and Luengnaruemitchai, A. (2018) Effect of the exposed ceria morphology on the catalytic activity of gold/ceria catalysts for the preferential oxidation of carbon monoxide. *Chemical Engineering Journal*, **344**, 545–555.

29. Lakshmanan, P., Delannoy, L., Richard, V., Méthivier, C., Potvin, C. and Louis, C. (2010) Total oxidation of propene over $Au/xCeO_2$-Al_2O_3 catalysts: Influence of the CeO_2 loading and the activation treatment. *Applied Catalysis B: Environment and Energy*, **96**, 117–125.

30. Galvagno, S. and Parravano, G. (1978) Chemical reactivity of supported gold. IV. Reduction of nitric oxide by hydrogen. *Journal of Catalysis*, **55**, 178–190.

31. Huang, P., Wu, F., Zhu, B., Gao, X., Zhu, H., Yan, T., Huang, W., Wu, S. and Song, D. (2005) CeO_2 nanorods and gold nanocrystals supported on CeO_2 nanorods as catalyst. *Journal of Physical Chemistry B*, **109**, 19169–19174.

32. Fandi, Z., Ameur, N., Brahimi, F. T., Bedrane, S. and Bachir, R. (2020) Photocatalytic and corrosion inhibitor performances of CeO_2 nanoparticles decorated by noble metals: Au, Ag, Pt. *Journal of Environmental Chemical Engineering*, **8**, 104346–104361.

33. Hossain, M. S. and Ahmed, S. (2023) FTIR spectrum analysis to predict the crystalline and amorphous phases of hydroxyapatite: a comparison of vibrational motion to reflection. *RSC Advances*, **13**, 14625–14630.

34. Girija, D., Naik, H. S. B., Sudhamani, C. and Kumar, B. V. (2011) Cerium oxide nanoparticles-a green, reusable, and highly efficient heterogeneous catalyst for the synthesis of polyhydroquinolines under solvent-free conditions. *Archives of Applied Science Research*, **3**, 373–382.

35. Bae, S., Gim, S., Kim, H. and Hanna, K. (2016) Effect of $NaBH_4$ on properties of nanoscale zero-valent iron and its catalytic activity for reduction of *p*-nitrophenol. *Applied Catalysis B: Environmental*, **182**, 541–549.

36. Kotp, M. G., El-Mahdy, A. F. and Kuo, S. -W. (2024) Rational decoration of porous organic polymers with silver nanoparticles for strategic reduction of hazardous nitroaryl compounds. *Polymer Chemistry*, **1**, 1–10.

37. Wu, B., Zhang, H., Chen, C., Lin, S. and Zheng, N. (2009) Interfacial activation of catalytically inert Au (6.7 nm)-Fe_3O_4 dumbbell nanoparticles for CO oxidation. *Nano Research*, **2**, 975–983.

38. Zhang, Y., Zhao, S., Feng, J., Song, S., Shi, W., Wang, D. and Zhang, H. (2021) Unraveling the physical chemistry and materials science of CeO_2-based nanostructures. *Chemistry*, **7**, 2022–2059.

39. Kadja, G. T., Ilmi, M. M., Azhari, N. J., Khalil, M., Fajar, A. T., Makertihartha, I., Gunawan, M. L., Rasrendra, C. B. and Wenten, I. (2022) Recent advances on the nanoporous catalysts for the generation of renewable fuels. *Journal of Materials Research and Technology*, **17**, 3277–3336.

40. Shanmugaraj, K., Bustamante, T. M., Torres, C. C. and Campos, C. H. (2022) Gold nanoparticles supported on mesostructured oxides for the enhanced catalytic reduction of 4-nitrophenol in water. *Catalysis Today*, **388**, 383–393.

41. Seo, Y., Ahn, E., Park, J., Kim, T., Hong, J., Kim, K., Park, Y. and Park, Y. (2017) Catalytic reduction of 4-nitrophenol with gold nanoparticles synthesized by caffeic acid. *Nanoscale Research Letters*, **12**, 1–11.

42. Yazid, H., Adnan, R., Farrukh, M. A. and Hamid, S. A. (2011) Synthesis of Au/Al_2O_3 nanocatalyst and its application in the reduction of *p*-nitrophenol. *Journal of the Chinese Chemical Society*, **58**, 593–601.